CHEMISTRY OF MATERIALS
Article

Chem. Mater. **2011,** *23,* 57–66 57
DOI:10.1021/cm102376b

CeO_2/Pt Catalyst Nanoparticle Containing Carbide-Derived Carbon Composites by a New In situ Functionalization Strategy

Emanuel Kockrick,*[,†,‡] Lars Borchardt,[†] Christian Schrage,[†] Cyril Gaudillere,[‡] Christoph Ziegler,[§] Thomas Freudenberg,[⊥] David Farrusseng,[‡] Alexander Eychmüller,[§] and Stefan Kaskel*[,†]

[†]*Department of Inorganic Chemistry, Dresden University of Technology (TU-Dresden), Mommsenstrasse 6, D-01062 Dresden, Germany,* [‡]*Institut de Recherche sur la Catalyse et l'Environnement de Lyon (IRCELYON) University Lyon 1, CNRS, 2, Avenue Albert Einstein, 69626 Villeurbanne, France,* [§]*Department of Physical Chemistry, Dresden University of Technology (TU-Dresden), Bergstrasse 66b, 01062 Dresden, Germany, and* [⊥]*Leibniz Institute for Solid State and Materials Research Dresden, Helmholtzstrasse 20, D-01069 Dresden, Germany*

Received April 5, 2010. Revised Manuscript Received October 23, 2010

A new class of CeO_2/Pt nanostructures containing highly porous carbide-derived carbon composites was obtained for the first time using a polymer precursor strategy and subsequent ceramization. The catalytic transition metal compounds were incorporated into polymeric polycarbosilane structures using an inverse microemulsion method in precisely tunable nanoscale particle sizes. Porous ceramic and carbon composites were obtained by pyrolysis and subsequent chlorination processes. The adsorption properties of nonoxidic ceramic intermediates can be adjusted by the pyrolysis temperatures from mainly microporous to meso- and macroporous materials, respectively. These pore structures remain during the chlorination process confirmed by comparative nitrogen physisorption and small-angle X-ray scattering investigations. The specific surface areas significantly increase up to 1774 m^2/g after selective silicon removal. In comparison to unsupported CeO_2/Pt nanoparticle structures, the particle sizes and dispersion of the active metal compounds of composite structures remain during pyrolysis and chlorination process studied by electron microscopy methods. Ceramic and carbonaceous composites show catalytic activity and stability in selective methane oxidation. In contrast to the SiC composites, the CDC materials promote the formation of carbon monoxide and hydrogen in reforming reactions at higher temperatures, a conversion pathway important for the generation of synthetic fuels.

Introduction

Micro- and mesostructured carbon materials attend considerable attention due to outstanding adsorption properties, high chemical and hydrothermal stability and good biocompartibility.[1−4] Therefore, these materials were extensively studied as sorbents, energy storage materials for hydrogen and hydrocarbon storage, respectively, and as catalyst and biomaterial supports.[5] Beside active carbon structures the syntheses of ordered mesoporous carbon materials were extensively studied in the past decade.[6−8] In comparison to a classical synthesis strategy, the mesopore size and symmetry can be precisely controlled by the ordered mesoporous exotemplate and the carbon precursor.[9,10] Incorporating noble metals like palladium and platinum or magnetic functionalization by in situ or ex situ loading resulting composites can be used as advanced heterogeneous catalyst systems in selective oxidation and hydrogenation reactions.[11−13]

In comprehensive studies, a new class of advanced carbon materials was introduced and synthesized by chlorination of various carbide systems.[14−17] The resulting carbide derived carbons (CDC) offer very adjustable micropore diameters and high specific surface areas and

*Corresponding author. E-mail: emanuel.kockrick@googlemail.com (E.K.); stefan.kaskel@chemie.tu-dresden.de (S.K.). Phone: +33 472 445 469 (E.K.); 49-351-46333632 (S.K.). Fax: +33 94 72 44 53 99 (E.K.); 49-351-46337287 (S.K.).

(1) Davis, M. E. *Nature* **2002**, *417*, 813.
(2) Joo, S. H.; Choi, S. J.; Oh, I.; Kwak, J.; Liu, Z.; Terasaki, O.; Ryoo, R. *Nature* **2001**, *412*, 169.
(3) Kruk, M.; Dufour, B.; Celer, E. B.; Kowalewski, T.; Jaroniec, M.; Matyjaszewski, K. *J. Phys. Chem. B* **2005**, *109*, 9216.
(4) Liang, C. D.; Dai, S. *J. Am. Chem. Soc.* **2006**, *128*, 5316.
(5) Yang, Z. X.; Xia, Y. D.; Mokaya, R. *J. Am. Chem. Soc.* **2007**, *129*, 1673.
(6) Jun, S.; Joo, S. H.; Ryoo, R.; Kruk, M.; Jaroniec, M.; Liu, Z.; Ohsuna, T.; Terasaki, O. *J. Am. Chem. Soc.* **2000**, *122*, 10712.
(7) Lee, K. T.; Ji, X. L.; Rault, M.; Nazar, L. F. *Angew. Chem., Int. Ed.* **2009**, *48*, 5661.
(8) Ryoo, R.; Joo, S. H.; Jun, S. *J. Phys. Chem. B* **1999**, *103*, 7743.
(9) Lu, A. H.; Schueth, F. *Adv. Mater.* **2006**, *18*, 1793.
(10) Ryoo, R.; Joo, S. H.; Kruk, M.; Jaroniec, M. *Adv. Mater.* **2001**, *13*, 677.
(11) Lu, A. H.; Li, W. C.; Hou, Z. S.; Schueth, F. *Chem. Commun.* **2007**, 1038.
(12) Lu, A. H.; Li, W. C.; Kiefer, A.; Schmidt, W.; Bill, E.; Fink, G.; Schueth, F. *J. Am. Chem. Soc.* **2004**, *126*, 8616.
(13) Lu, A. H.; Schmidt, W.; Matoussevitch, N.; Bonnemann, H.; Spliethoff, B.; Tesche, B.; Bill, E.; Kiefer, W.; Schueth, F. *Angew. Chem., Int. Ed.* **2004**, *43*, 4303.
(14) Dash, R. K.; Nikitin, A.; Gogotsi, Y. *Microporous Mesoporous Mater.* **2004**, *72*, 203.
(15) Dash, R. K.; Yushin, G.; Gogotsi, Y. *Microporous Mesoporous Mater.* **2005**, *86*, 50.

Published on Web 12/10/2010

pore volumes, respectively.[18] Thus, these CDC structures are potential candidates as gas storage materials with outstanding hydrogen and hydrocarbon capacities or for super capacitor and for biological applications.[19−24] However, there are only a few reports for the preparation of hierarchically structured CDC materials containing micro- and mesopore systems that are beneficial for catalytic applications.[25−27] In different studies, the influence of various transition metals (e.g., platinum and ruthenium) were investigated on the structure and sorption properties of resulting CDC materials.[28−31]

In the following, we introduce a polymer precursor strategy for the preparation of highly porous CDC composites containing nanoscale, catalytically active CeO_2/Pt species. Nanoscale cerium dioxide is an interesting catalyst system for total oxidation processes of soot and methane and carbon monoxide because of good oxygen donation and the high surface to volume ratio.[32−35] In combination with other noble transition metals like Pt, Au, Cu, doped nanoscale catalyst systems offer high activity in water gas shift reaction and denitrification with hydrocarbons (HC-SCR, hydrocarbon selective catalytic reduction).[36,37] However, because sintering and particle aggregation processes occur at the elevated temperatures catalyst performance is lowered over several reaction cycles.[38] Therefore, the incorporation into thermally stable and inert matrices is requested. Nevertheless, post functionalization of porous matrices often leads to a weak template to catalyst interaction and high mobility of active species. In contrast, the direct incorporation of molecular metal compounds during the formation of the porous matrix generates a high dispersion and good chemical and thermal stability.[39] Thus, from environmental and economic aspects the direct functionalization strategy demonstrates several advantages. In recent studies, we observed the applicability of inverse microemulsions for the direct incorporation of highly dispersed, functional nanostructures into polymeric and ceramic systems.[40−42] The particle size of catalytic, luminescent, or photochromic particles can be precisely tuned within a few nanometers by the molar water to surfactant ratio (R_W value) of micellar nanoreactor system.[38,43,44]

The schematic synthesis strategy of CeO_2/Pt-CDC (CDC-X) composites is presented in Scheme 1. The polymeric CeO_2/Pt-PCS (PCS) composites with a defined ceria and platinum content were prepared by an inverse microemulsion method and the ceramic CeO_2/Pt-SiC (SiC-X) materials were obtained by subsequent pyrolysis (Scheme 1, first step) at 1200 °C (SiC-1), 1350 °C (SiC-2), and 1500 °C (SiC-3), respectively. These synthesis were already reported by our group in earlier studies.[41] To remove residual carbon formed during the carbonization of organic compounds (e.g., surfactant), several ceramic materials were oxidized at 700 °C (Scheme 1, second step). Carbide-derived carbon composites (CDC-X) were synthesized by chlorination in a conventional tubular furnace at 1000 °C for 3 h and using an infrared furnace (1000 °C, 0.5 h, CDC-2-IR) with ultrafast heating ramps (Scheme 1, third step). The latter IR equipment was already successfully employed for the preparation of ordered mesoporous carbide derived carbon and intermetallic CMK-3 composites.[45,46] Trapped chlorine was removed by reductive treatment at 600 °C and subsequent calcination process at 80 °C to reactivate the ceria species (Scheme 1, fourth step, CDC-2-IR-H). The catalytic activity of elevated silicon carbide and carbon composites were investigated in selective methane oxidation.

Experimental Section

All chemicals were used as received.

Synthesis of CeO_2/Pt-CDC Composites. Porous ceria and platinum containing polycarbosilane (PCS) and ceramic composites

(16) Gogotsi, Y.; Dash, R. K.; Yushin, G.; Yildirim, T.; Laudisio, G.; Fischer, J. E. *J. Am. Chem. Soc.* **2005**, *127*, 16006.
(17) Gogotsi, Y.; Nikitin, A.; Ye, H. H.; Zhou, W.; Fischer, J. E.; Bo, Y.; Foley, H. C.; Barsoum, M. W. *Nat. Mater.* **2003**, *2*, 591.
(18) Yushin, G.; Dash, R.; Jagiello, J.; Fischer, J. E.; Gogotsi, Y. *Adv. Funct. Mater.* **2006**, *16*, 2288.
(19) Chmiola, J.; Largeot, C.; Taberna, P. L.; Simon, P.; Gogotsi, Y. *Angew. Chem., Int. Ed.* **2008**, *47*, 3392.
(20) Chmiola, J.; Yushin, G.; Gogotsi, Y.; Portet, C.; Simon, P.; Taberna, P. L. *Science* **2006**, *313*, 1760.
(21) Gogotsi, Y.; Dash, R. K.; Yushin, G.; Carroll, B. E.; Altork, S. R.; Sassi-Gaha, S.; Rest, R. F. *J. Biomed. Mater. Res., Part A* **2008**, *84A*, 607.
(22) Yeon, S. H.; Osswald, S.; Gogotsi, Y.; Singer, J. P.; Simmons, J. M.; Fischer, J. E.; Lillo-Rodenas, M. A.; Linares-Solanod, A. *J. Power Sources* **2009**, *191*, 560.
(23) Yushin, G.; Hoffman, E. N.; Barsoum, M. W.; Gogotsi, Y.; Howell, C. A.; Sandeman, S. R.; Phlllips, G. J.; Lloyd, A. W.; Mikhalovsky, S. V. *Biomaterials* **2006**, *27*, 5755.
(24) Korenblit, Y.; Rose, M.; Kockrick, E.; Borchardt, L.; Kvit, A.; Kaskel, S.; Yushin, G. *ACS Nano* **2010**, *4*, 1337.
(25) Krawiec, P.; Kockrick, E.; Borchardt, L.; Geiger, D.; Corma, A.; Kaskel, S. *J. Phys. Chem. C* **2009**, *113*, 7755.
(26) Yeon, S.-H.; Reddington, P.; Gogotsi, Y.; Fischer, J. E.; Vakifahmetoglu, C.; Colombo, P. *Carbon* **2010**, *48*, 201.
(27) Oschatz, M.; Kockrick, E.; Rose, M.; Borchardt, L.; Klein, N.; Senkovska, I.; Freudenberg, T.; Korenblit, Y.; Yushin, G.; Kaskel, S. *Carbon* **2010**, *48*, 3987.
(28) Ersoy, D. A.; McNallan, M. J.; Gogotsi, Y. *J. Electrochem. Soc.* **2001**, *148*, C774.
(29) Leis, J.; Perkson, A.; Arulepp, M.; Nigu, P.; Svensson, G. *Carbon* **2002**, *40*, 1559.
(30) Kormann, M.; Gerhard, H.; Zollfrank, C.; Scheel, H.; Popovska, N. *Carbon* **2009**, *47*, 2344.
(31) Glenk, F.; Knorr, T.; Schirmer, M.; Gutlein, S.; Etzold, B. J. M. *Chem. Eng. Technol.* **2010**, *33*, 698.
(32) Bera, P.; Gayen, A.; Hegde, M. S.; Lalla, N. P.; Spadaro, L.; Frusteri, F.; Arena, F. *J. Phys. Chem. B* **2003**, *107*, 6122.
(33) Liu, W.; Flytzani-Stephanopoulos, M. *J. Catal.* **1995**, *153*, 317.
(34) Trovarelli, A. *Catal. Rev., Sci. Eng.* **1996**, *38*, 439.
(35) Yao, H. C.; Yao, Y. F. Y. *J. Catal.* **1984**, *86*, 254.
(36) Fu, Q.; Saltsburg, H.; Flytzani-Stephanopoulos, M. *Science* **2003**, *301*, 935.
(37) Fu, Q.; Weber, A.; Flytzani-Stephanopoulos, M. *Catal. Lett.* **2001**, *77*, 87.
(38) Kockrick, E.; Schrage, C.; Grigas, A.; Geiger, D.; Kaskel, S. *J. Solid State Chem.* **2008**, *181*, 1614.
(39) Krawiec, P.; Kockrick, E.; Auffermann, G.; Simon, P.; Kaskel, S. *Chem. Mater.* **2006**, *18*, 2663.
(40) Althues, H.; Henle, J.; Kaskel, S. *Chem. Soc. Rev.* **2007**, *36*, 1454.
(41) Kockrick, E.; Frind, R.; Rose, M.; Petasch, U.; Boehlmann, W.; Geiger, D.; Herrmann, M.; Kaskel, S. *J. Mater. Chem.* **2009**, *19*, 1543.
(42) Kockrick, E.; Krawiec, P.; Petasch, U.; Martin, H.-P.; Herrmann, M.; Kaskel, S. *Chem. Mater.* **2008**, *20*, 77.
(43) Dresco, P. A.; Zaitsev, V. S.; Gambino, R. J.; Chu, B. *Langmuir* **1999**, *15*, 1945.
(44) Henle, J.; Simon, P.; Frenzel, A.; Scholz, S.; Kaskel, S. *Chem. Mater.* **2007**, *19*, 366.
(45) Kockrick, E.; Schmidt, F.; Gedrich, K.; Rose, M.; George, T. A.; Skomski, R.; Kaskel, S. *Chem. Mater.* **2010**, *22*, 1624.
(46) Kockrick, E.; Schrage, C.; Borchardt, L.; Klein, N.; Rose, M.; Senkovska, I.; Kaskel, S. *Carbon* **2010**, *48*, 1707.

Scheme 1. Synthesis Strategy for the Preparation of CeO_2/Pt Containing Polymeric PCS, Ceramic SiC-X and Carbonaceous CDC-X Composites, Respectively, Synthesized by Inverse Microemulsion Method and Subsequent Pyrolysis and Chlorination Treatment

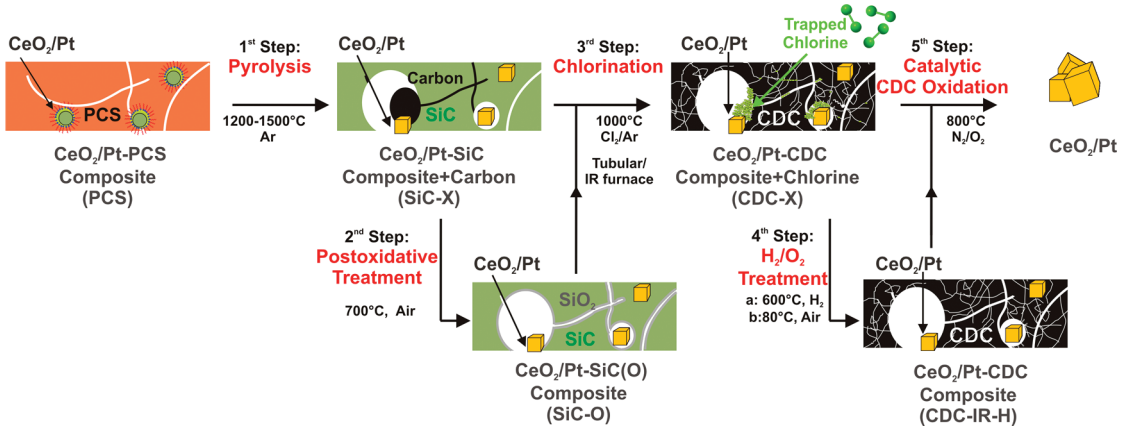

(SiC-X) with a theoretical Pt mass content of 0.7 wt % were synthesized according to our previous studies.[41] Metal-containing, carbide-derived carbon composites (CDC-X) were prepared via chlorination of silicon carbide composites (SiC-X) at 1000 °C. In the typical procedure, 500 mg of SiC-X material was heated in a quartz boat inside quartz tube in horizontal tubular furnace in 30 mL min^{-1} argon flow to desired temperature (450 °C h^{-1}). Afterward, Cl_2 was introduced for 3 h (30 mL min^{-1} flow) while the argon flow was maintained at the same level. After that time, Cl_2 was switched off and the product was cooled to room temperature in an argon flow.[25] In comparison, CDC-2-IR material chlorinated in IR furnace (Behr IRF 10) was first flushed in argon flow for 1 h in a quartz boat inside quartz tube. Afterward, chlorine (30 mL min^{-1} flow) was introduced at room temperature and then SiC-X was heated to 1000 °C (3 °C s^{-1}) for 30 min. After the chlorination process, resulting carbon materials were cooled in an argon flow.[46] Residual chlorine was removed by post-reductive treatment in hydrogen flow. In a typical procedure, 200 mg of CDC-2-IR was heated in a quartz boat inside quartz tube in IR furnace in 30 mL min^{-1} H_2 flow to 600 °C for 30 min (3 °C s^{-1}). In the last step, H_2-treated carbon structures were annealed at 80 °C for 2 h under static air atmosphere in order to activate active metal compounds (CDC-2-IR-H).

Ceria and platinum reference materials were prepared by separate addition of an excess of concentrated ammonia solution to aqueous cerium nitrate (0.2 mol L^{-1}) and hexachloro platinic acid solution (0.2 mol L^{-1}), subsequent filtration and washing steps of precipitation. Afterward the precipitates were calcined at 600 °C for 1 h. The nanoscalic reference systems were chlorinated according to above-described procedure at 1000 °C in IR furnace. The ordered mesoporous reference material (OM-CDC) for thermogravimetric measurements was synthesized by nanocasting strategy and subsequent chlorination at 1000 °C. The detailed synthesis conditions can by found in earlier studies.[25,46]

Characterization. Nitrogen and hydrogen physisorption isotherms were measured at −196 °C using a Quantachrome Autosorb 1c apparatus. Prior to the measurement, the samples were degassed in vacuum at 150 °C for 24 h. Specific surface areas were calculated using the BET equation (p/p_o = 0.05−0.2). The pore size distribution was estimated according to the QSDFT equilibrium model (QSDFT, quenched solid density functional theory, for slit pores) using the Autosorb 1.56 software from Quantachrome. The specific micropore volume was also calculated by the above-mentioned DFT model. Small-angle X-ray scattering (SAXS) experiments were performed on a Bruker Nanostar (sealed tube, Cu Kα; 1.51406 Å) with a position-sensitive HiStar detector. The sample to detector distance was 25 and 105 cm, respectively, to cover a q-range from 0.03 to 0.84 $Å^{-1}$ ($q = 4\pi\sin\Theta/\lambda$). The scattering data obtained from different measurement distances was combined after transmission-weighted background subtraction. Wide-angle X-ray powder diffraction patterns were recorded in transmission geometry using a Stoe Stadi−P diffractometer and Cu $K\alpha_1$ radiation (λ = 0.15405 nm). Size broadening of reflections in the range from 2θ = 20−90° was analyzed using the Stoe size/strain analysis. Instrumental broadening was taken into account based on LaB_6 reference measurements. FESEM (field-emission scanning electron microscopy) and elemental mapping investigations on metal containing polymer, cermic and carbon composites was carried out with a Stereoscan 260 SEM with EDX analysis system using SE (secondary electrons) and BSE (backscattered electrons) detectors, respectively. Elemental analyses using EDX were obtained as a mean value of five measurements in a magnification of 3000. Samples for TEM analysis were prepared by dipping carbon coated copper grids into an ethanol suspension of CeO_2/Pt-CDC composites. TEM investigations were performed on a 200 kV TEM FEI Tecnai T20 instrument. A Netzsch STA-409 instrument was used for thermal analyses. The carbon systems were heated in a corundum crucible up to 800 °C with 10 °C/min in air atmosphere. The platinum, cerium, and silicon contents were estimated using an ICP-OES spectrometer with CCD detector and radially viewed plasma system (Varian). Raman spectra were obtained on a Renishaw RM-2000 Raman microscope using a 532 nm Laser (Gem532 from Laser Quantum) as the excitation source. The Laser was focused through a 50x objective to about 2 μm in diameter. To prevent thermal degradation, the power was kept below 0.6 mW on the sample. Measurements were performed in backscattering geometry in a range from 500 to 3200 cm^{-1} with 60 s exposure time. Data fitting and evaluation was done with the Wire 2.0 Software from Renishaw.

Catalytic tests were carried out on the Switch 16 parallel reactor (AMTEC GmbH−CNRS) as described in previous studies by Morra et al.[47] This multichannel device consists of 16 parallel reactors in Inconel with two independent feeding systems. In this study, the switching 16 port valve allows us to

(47) Morra, G.; Desmartin-Chomel, A.; Daniel, C.; Ravon, U.; Farrusseng, D.; Cowan, R.; Krusche, A.; Mirodatos, C. *Chem. Eng. J.* **2008**, *138*, 379.

(i) regenerate catalysts under air after gas chromatography (GC) sampling is achieved and (ii) perform unsteady state testing by switching the feed from air to methane and recording online. Reaction gases were analyzed by gas chromatography (GC HP 6950 and 6980). Prior catalytic runs, catalysts were degassed at 250 °C for 48 h under inert helium flow. When the targeted reaction temperature is reached, the downstream is analyzed in an empty reactor in order to measure blank activity. One reactor is then fed by the inlet stream while the 15 reactors are remaining under inert helium flow (50 mL/min) conditions. The first GC analysis is carried out after 5 min of time on stream and second one after 17 min to investigate possible rapid deactivation processes. Reported values correspond to the average of these two analyses. A subsequent reactor is then selected for a catalytic run. After all runs are completed at a given temperature, the temperature is heated up to the next plateau, from 250 to 500 °C every 25 °C at atmospheric pressure.

Results and Discussion

The material properties and catalytic performance of polymer, ceramic and carbonaceous composite materials were characterized by various methods that are summarized in the following sections: After discussion of gas physisorption and small-angle X-ray scattering results the microscopy and structural investigations are presented. Finally, the performance of elevated SiC and CDC composites as catalyst systems in selective methane oxidation is introduced.

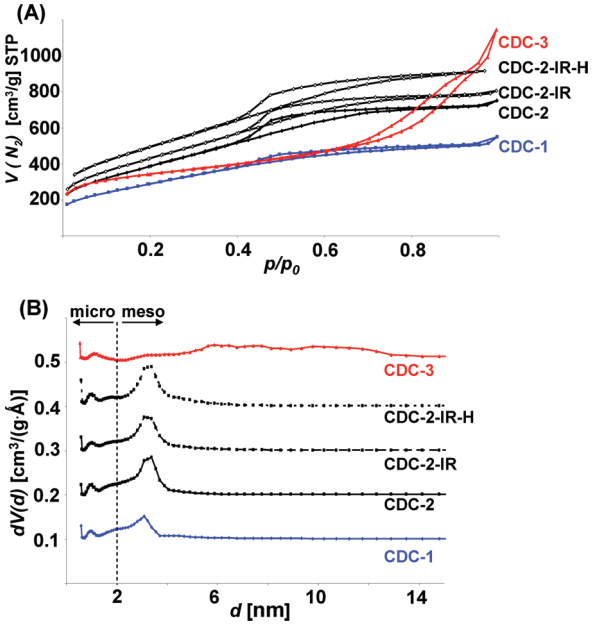

Figure 1. (A) Nitrogen physisorption isotherms of polymeric (PCS), ceramic (SiC-X), and carbonaceous composites (CDC-X) prepared at different pyrolysis and chlorination conditions and (B) corresponding pore size distributions for CDC-X composites estimated by QSDFT methods.

Physisorption. The adsorption properties of porous composite materials were investigated by nitrogen physisorption measurements and are summarized in Figure 1 and Table 1. The results for polymer (PCS) and ceramic composites (SiC-X) with a theoretical platinum content of 0.7 wt % were already discussed more detailed in our previous investigations.[41] According to the nitrogen physisorption isotherms, the specific surface areas, pore sizes, and volumes, respectively, of CDC-X composites (Scheme 1, third step) are strongly dependent on the pyrolysis temperatures (Scheme 1, first step). In agreement with our former studies, the specific surface area decreases with higher pyrolysis temperature, which is ascribed to stronger sintering processes at 1350 and 1500 °C.[48] At constant chlorination conditions, the specific surface area increases with rising pyrolysis temperature from 1051 m^2/g at 1200 °C up to 1406 m^2/g at 1350 °C. A further increase up to 1500 °C causes a drop to 1205 m^2/g. In comparison to polymer and ceramic composites, the surface area increases significantly from 537 m^2/g (PCS) and 116 m^2/g (SiC-2) up to 1406 m^2/g (CDC-2). The latter can be explained by selective silicon removal due to the chlorination process forming highly porous carbide-derived carbon structures. In comprehensive studies, the influence of postoxidative treatment of ceramic composites was studied (Scheme 1, second step) because these materials offer significantly higher surface areas (SiC-1-O: 409 m^2/g) compared to pyrolyzed ones (SiC-1, 251 m^2/g).[41] However, the resulting CDC materials are less porous (CDC-1-O, 933 m^2/g). This can be explained by the partial oxidation (silicon oxycarbides) and surface passivation (silica layer) of porous silicon carbide matrix during postoxidative treatment causing a higher silicon content in carbide derived carbons due to the incomplete silicon removal. Thus, further discussions are focused on the direct chlorination of pyrolyzed ceramic composites. Additionally, the effect of shorter chlorination duration using an infrared furnace for 30 min and ultrafast heating ramps (3 °C/s) was investigated for ceramic composites pyrolyzed at 1350 °C. In contrast to our previous studies on the synthesis of ordered mesoporous CDC materials, specific surface area of resulting CDC composites increases

Table 1. Sample Codes and Adsorption Properties of Metal-Containing SiC-X and CDC-X composites Dependent on the Pyrolysis and Chlorination Conditions

CDC-	$T_{Pyrolysis}$ (°C)	$T_{Chlorination}$ (°C)	$S_{g,SiC}$[d] (m^2/g)	$S_{g,CDC}$[d] (m^2/g)	V_{mic}[e] (cm^3/g)	V_{tot}[f] (cm^3/g)	H_2[g] (gew%)
1	1200	1000	251	1051	0.32	0.80	0.89
1-O[a]	1200	1000	409	933	0.27	0.68	0.81
2	1350	1000	116	1406	0.39	1.13	1.22
2-IR[b]	1350	1000 IR	116	1565	0.45	1.23	1.39
2-IR-H[c]	1350	1000 IR	116	1774	0.53	1.41	1.79
3	1500	1000	129	1205	0.38	1.54	1.29

[a] Postsynthetic oxidation of pyrolyzed ceramic at 700 °C. [b] Chlorinatin in IR furnace. [c] Postsynthetic reduction oxidation of CDC composites. [d] Estimated at $p/p_0 = 0.05-0.2$. [e] Micropore volume ($d < 2$ nm) estimated by QSDFT method for N_2 at 77 K. [f] Total volume calculated at $p/p_0 = 0.98$. [g] Volumetric H_2 capacity at 77 K and 1 bar.

up to 1565 m^2/g (CDC-2-IR) compared to treatment in regular tube furnace (CDC-2, 1406 m^2/g).[46] To remove residual chlorine, we further treated this composite material under reductive hydrogen conditions and subsequently calcined it at 150 °C to reactivate the CeO_2 compound (Scheme 1, fourth step). This purification process causes a noteworthy gain in surface area up to 1774 m^2/g.

Similar tendencies were also observed for specific pore volumes of CDC-X composites. However, comparable micropore volumes of 0.32−0.39 cm^3/g were obtained for chlorination treatment in regular furnace, whereas the total pore volume rises from 0.80 to 1.54 cm^3/g with increasing pyrolysis temperature. The latter indicates a larger mesopore and interparticular content at 1350 and 1500 °C, respectively. This can be attributed to the lower carbon content of carbonized surfactants at higher pyrolysis temperatures in composite ceramics.[41] Because of auto-oxidation processes taking place at higher pyrolysis temperatures, this mesopore blocking carbon is removed increasing the pore volume and specific surface areas of ceramic and CDC composites

Shorter chlorination duration and subsequent purification processes effect a considerable augmentation up to 0.53 and 1.79 cm^3/g. Corresponding pore size distributions for CDC composites (Figure 1B) show a bimodal pore size distributions for carbon materials with comparable micropore diameters in the range of 0.7−1.5 nm. However, the mesoscopic pore size distribution is strongly dependent on the pyrolysis temperature, because composites annealed at 1200 and 1350 °C offer narrow pore sizes in the range of 2−5 nm. In contrast, a broad distribution results for 1500 °C. Interestingly, the mesoscopic pore structure remains during chlorination because similar isotherm shapes and pore size distributions (Figure 1 and Supporting Information 1) were observed for ceramic and carbon composites pyrolyzed at a constant temperature. The latter demonstrates the efficiency of applied endotemplating synthesis strategy for the preparation of mesostructured carbide-derived carbon materials.

Hydrogen physisorption measurements of CDC-X composites at −196 °C show similar tendencies to above-described nitrogen methods (Table 1, ESI 2). Storage capacities at 1 bar increase with increasing pyrolysis temperature from 0.86 wt % (CDC-1) to 1.29 wt %. (CDC-3). Shorter chlorination duration and purification treatment generate composites with hydrogen uptakes to 1.79 wt % (CDC-2-IR-H). The received CDC-X composites offer similar H_2 uptakes compared to microporous CDC materials obtained by chlorination of bulk SiC. But they are lower than mesostructured CDC materials synthesized by exotemplating strategy.[25]

Small-Angle X-ray Scattering. To complete the structural information obtained by physisorption measurements, we carried out small-angle X-ray studies. Figure 2 shows SAXS data of the pyrolyzed and chlorinated samples in a log I vs log q plot. The CDC reference material is characterized by a typical trend for microporous carbon showing two linear regimes with a certain slope, divided by a decreasing curvature at median q values. To quantify this characteristic profile found in various porous carbon materials, we can apply the following analytical expression proposed by Kalliat et al.[49] and modified by Gibaud et al.[50] (eq 1). An additional summand (with parameters B_2 and $R_{G,2}$) is introduced to evaluate the bimodal pore size distribution present in the examined samples.[46]

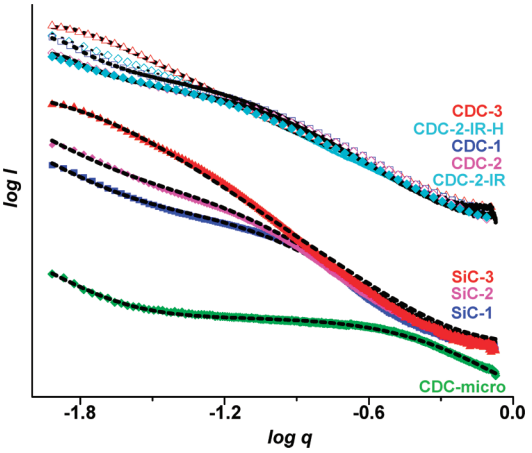

Figure 2. Small-angle scattering graphs and peak fittings of ceramic SiC-X and carbonaceous CDC-X composites and microporous CDC reference material (CDC-micro), respectively.

$$I(q) = \frac{A}{q^n} + \frac{B_1}{\left(\frac{6}{R_{G,1}^2} + q^2\right)^2} + \frac{B_2}{\left(\frac{6}{R_{G,2}^2} + q^2\right)^2} + C \quad (1)$$

The first term describes the scattering contribution of an external surface or pores with dimensions larger 10 nm and dominates the scattering function at low q. If ideal POROD behavior is assumed the exponent n is close to 4 indicating a smooth surface.[51] Variations toward smaller n suggest the presence of surface asperities in the range of $2\pi q^{-1}$(fractal behavior). Although the parameter C reflects a constant background, the second and third term offers information about pores in two different size regimes. Thus, radii of gyration reflect the pore size and parameters B_1 and B_2 corresponding to the surface area contributed by different pore classes. In our case, the parameters indexed with 1 belong to micropores obtained by chlorination of SiC, whereas terms labeled with 2 offer information about larger pores emerged from pyrolysis of polymerized SMP-10. The results of the curve fitting are shown together with scattering data in Figure 2 (dashed lines) revealing a good agreement of data fitting and experimental results although there is a slight difference of fitted data from experimental scattering

(48) Krawiec, P.; Schrage, C.; Kockrick, E.; Kaskel, S. *Chem. Mater.* **2008**, *20*, 5421.
(49) Kalliat, M.; Kwak, C. Y.; Schmidt, P. W. In *New Approaches in Coal Chemistry*; ACS Symposium Series; American Chemical Society: Washington, D.C., 1981; Vol. *169*.
(50) Gibaud, A.; Xue, J. S.; Dahn, J. R. *Carbon* **1996**, *34*, 499.
(51) Guinier, A.; Gerard, F., *Small-Angle Scattering of X-rays*; John Wiley & Sons: New York, 1955.

Table 2. Radii of Gyration and Fitting Parameters According to eq 1 of Reference Material and SiC-X and CDC-X Composites

	R_{G1} (nm)	R_{G2} (nm)	n	A	B_1	B_2
CDC reference	0.54		3.1	3.87×10^{-4}	1.52	
SiC-1	~0	2.7	3.0	0.039	~0	0.13
CDC-1	1.3	2.9	2.94	0.036	0.113	0.068
SiC-2	~0	3.8	3.0	0.131	~0	0.18
CDC-2	1.0	3.46	2.42	0.106	0.120	0.093
CDC-2-IR	0.82	3.01	2.46	0.100	0.139	0.054
CDC-2-IR-H	0.96	4.19	2.72	0.119	0.125	0.028
SiC-3	~0	14.1	2.8	0.260	~0	0.11
CDC-3	1.48	12.0	2.13	0.288	0.137	0.009

curves for pyrolyzed samples resulting from the more complex electron density profile of these samples.

The achieved fitting parameters are summarized in Table 2 confirming the increase of pore sizes together with a higher surface area contribution of larger pores when pyrolysis temperatures is increased (increasing R_{G2} and A values). This trend is in agreement with increasing total pore volume shown by physisorption results proving the assumption of coalescing pores with higher temperatures. Furthermore, it is apparent that smaller pores (< 2 nm) are not present for pyrolyzed samples reflected by the absence of R_{G1} and B_1 in data fitting. Pores originated from chlorination of pyrolyzed SMP-10 are in the size regime of 0.8−1.3 nm, which is a bit larger than micropores in a CDC reference material made by chlorination of bulk SiC. Referring to the low q exponent n the surface of chlorinated samples is characterized by higher roughness indicated by smaller n values, which is even more pronounced for CDC materials pyrolyzed at higher temperatures. No drastic differences in scattering characteristics are found for the reductive post-treated sample which exhibits highest surface area and H_2-capacity as well. The radius of gyration of larger pores within this sample is slightly increased to 4.2 nm because of the reductive post-treatment while the surface roughness is decreased ($n = 2.72$).

Microscopy and Structural Investigations. The microstructure of resulting composite materials after pyrolysis and chlorination treatment was investigated by electron microscopy methods and is presented in Figure 3 and Supporting Information 3. It is evident that the microstructure of SiC-X materials is strongly dependent on the pyrolysis conditions. However, the particle morphologies remain similar during the chlorination processes. The latter results show good agreement to already discussed nitrogen physisorption measurements because similar isotherm shapes were obtained for SiC and CDC composites pyrolyzed at a constant temperature. Additionally, the gain of adsorbed nitrogen volume at higher relative pressures for SiC-1500 and CDC-1500−1000 composites (Figure 1) can be explained by the small particle size (Supporting Information 3 G and H) causing interparticular capillary condensation and apparently broad pore size distribution. In comprehensive studies, element-specific mapping and energy-dispersive X-ray spectroscopy (EDX) experiments (Si, Ce, Pt) were carried out, demonstrating the efficiency of selective chlorination process because almost no silicon can be detected in all CDC composites (Supporting Information 4). In contrast, catalytic active platinum and cerium species remain in a high dispersion after pyrolysis and chlorination treatment (Figure 3). The stability of the metal species during the Cl_2 treatment show good agreement to studies of Gogotsi et al. on the chlorination of silicon carbide layers on a platinum sample holder.[28] The formation of highly dispersed Pt-layers within the carbide-derived carbon was explained by the low thermodynamical stability of gaseous platinum chlorides species at these conditions compared to the exergonic formation of gaseous silicon tetrachloride.

The EDX results were confirmed by TEM investigations, because no transition and lanthanide metal aggregates can be detected in the CDC composite (Figure 4 A, Supporting Information 5). In high resolution mode lattice spacings of 3.18 Å and 1.89 Å could be analyzed by FFT method (Figure 4 B) and correspond to the (111) and (220) d-spacings of CaF_2-type cerium dioxide. These size dimensions of 2−3 nm correspond to previous results for cerium hydroxide nanoparticles in starting microemulsion system and ceria nanoparticles incorporated in the cross-linked polycarbosilane matrix.[38,41] The latter results verify our synthesis concept for size control and preservation of nanoscale structures during thermal treatments using the inverse microemulsion technique in combination with cross-linking processes of appropriate matrix systems. However, no separate Pt structures were detected by TEM method. In our previous studies a higher activity of platinum containing CeO_2−SiC composites were observed in the methane combustion compared to CeO_2−SiC and Pt−SiC systems, respectively.[41] This indicates a direct ceria to platinum interaction. Because no elemental Pt particles were analyzed an ionic dispersion on the ceria crystallite surface can be assumed.[52] This hypothesis is confirmed by the studies of Bera et al. on the ionic dispersion of platinum- and palladium-doped ceria catalyst systems.[53,54]

Raman spectra of CDC materials show strong first-order D- and G-bands at ~1340 and ~1595 cm^{-1}, respectively (Figure 5). Additionally, two weak second-order combinations, 2D at ~2680 cm^{-1} and D+G at ~2930 cm^{-1}, have been observed. Yo deconvolute the spectra in the region from 1000 to 1800 cm^{-1}, we used a fitting procedure by Shimodaira and Masui.[55] The region was fitted with four mixed Gaussian/Lorenzian curves on top of a linear background. Therefore, all samples show two rather sharp peaks at 1600 ± 1 and 1338 ± 2 cm^{-1}, named G1 and D1, and two broader peaks at 1545 ± 1 and 1336 ± 4 cm^{-1}, named G2 and D2. Besides hardly changing positions of the bands, the fwhm (full width at

(52) Matolin, V.; Matolinova, I.; Vaclavu, M.; Khalakhan, I.; Vorokhta, M.; Fiala, R.; Pis, I.; Sofer, Z.; Poltierova-Vejpravova, J.; Mori, T.; Potin, V.; Yoshikawa, H.; Ueda, S.; Kobayashi, K. *Langmuir* **2010**, *26*, 12824.
(53) Bera, P.; Patil, K. C.; Jayaram, V.; Subbanna, G. N.; Hegde, M. S. *J. Catal.* **2000**, *196*, 293.
(54) Bera, P.; Priolkar, K. R.; Gayen, A.; Sarode, P. R.; Hegde, M. S.; Emura, S.; Kumashiro, R.; Jayaram, V.; Subbanna, G. N. *Chem. Mater.* **2003**, *15*, 2049.
(55) Shimodaira, N.; Masui, A. *J. Appl. Phys.* **2002**, *92*, 902.

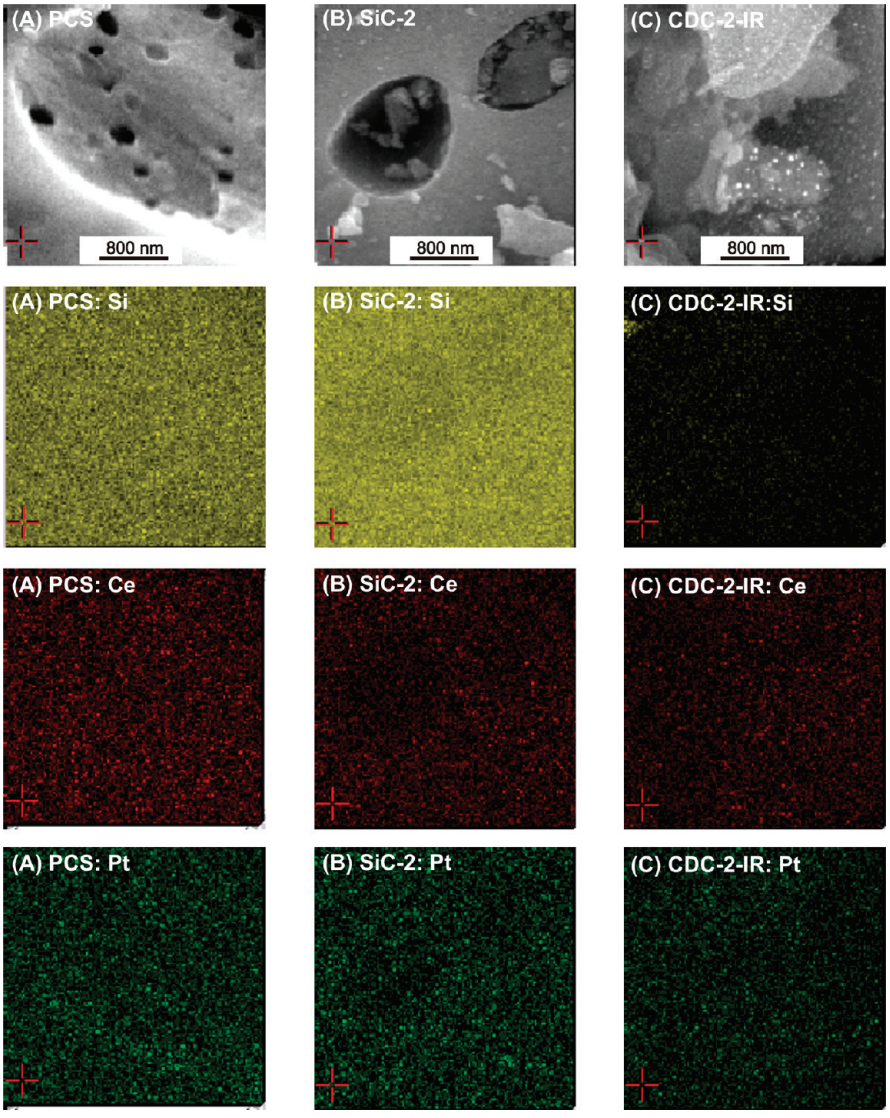

Figure 3. Field-emission scanning electron microscopy and elemental specific mapping investigations (Si, Ce, Pt) of polymeric PCS, ceramic SiC-2, and carbonaceous CDC-2-IR composites.

half-maximum) also barely changes for different samples. The fwhm are 64 ± 1 cm^{-1} for the G1 band, 105 ± 6 cm^{-1} for the G2 band, 76 ± 6 cm^{-1} for the D1 band, and 290 ± 15 cm^{-1} for the D2 band. Hence, one can state that the physicochemical character of the carbon in all CDC materials under consideration is comparable.

A more detailed discussion of the four bands leads to further understanding of their origin. The G1 and D1 peaks can be assigned to the in-plane stretching (like E_{2g}) and breathing (like A_{1g}) modes of winding short basal planes with bond angle order. The upshift of the G1 peak to higher wavenumbers, compared to the graphite value ($\sim$1580 cm^{-1}), could either be due to formation of graphite intercalation compounds, which is unlikely here, or be based on very small crystal sizes. Considering the I(D1)/I(G1) ratio, which varies from 1.2 to 1.6, the in-plane crystalline size L_a can be calculated to be between 3.6 and 2.7 nm, following the formula by Tuinstra an Koenig (Supporting Information 6).[56] The broader G2 and D2 bands are ascribed to sp^2 clusters with bond angle disorder like in amorphous carbon materials.[57] These clusters probably link the winding short basal planes.

All CDC carbon composites show X-ray amorphous structures although crystallinity of non oxidic matrix for SiC composites increases with higher pyrolysis temperatures. (Figure 6, ESI 7) For SiC-3 the cubic β-SiC phase was detected in agreement to previous investigations.[41,42] However, no crystalline ceria and platinum phase was observed for all polymer ceramic and carbon materials. For polymer and ceramic structures, this absence can be related to the low mass fraction and was discussed in prior studies. Additionally, the small particle sizes and low degree of crystallinity estimated by above-discussed electron microscopic methods cause the lack of diffraction signals for CDC composites. To evaluate the stability of oxidic and noble metal compounds during the chlorination process, we investigated the performance of pure ceria

(56) Tuinstra, F.; Koenig, J. L. *J. Chem. Phys.* **1970**, *53*, 1126.

(57) Yoshikawa, M.; Katagiri, G.; Ishida, H.; Ishitani, A.; Akamatsu, T. *J. Appl. Phys.* **1988**, *64*, 6464.

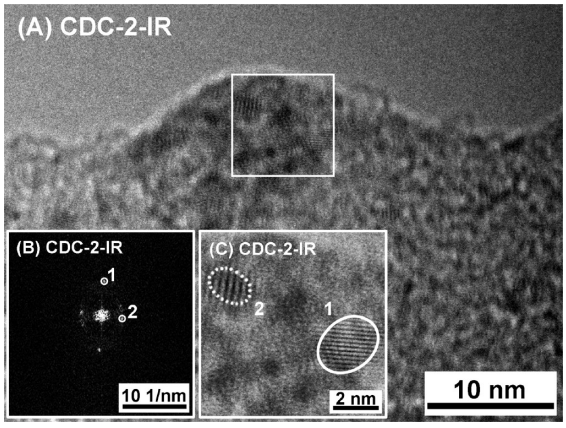

Figure 4. High-resolution bright-field micrograph of the catalyst nanoparticle containing carbide-derived carbon composites chlorinated in IR-furnace (CDC-2-IR-H). Weak lattice fringes are visible of the CeO_2/Pt nanoparticles in vertical and horizontal directions. The white square in image A indicates the region from which the FFT diffractogram was generated. Inset shows the FFT with clear spots indexed with numbers. The second inset C is the detail magnification of the white square from image A. The framed regions (dotted and continuous line) highlight the areas with lattice fringes. The numbers 1 and 2 correspond to the spots in the diffractogram and represent the area from which they originate.

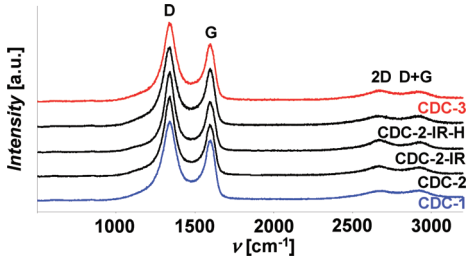

Figure 5. Raman spectra of CDC-X composites prepared at different thermal treatment conditions.

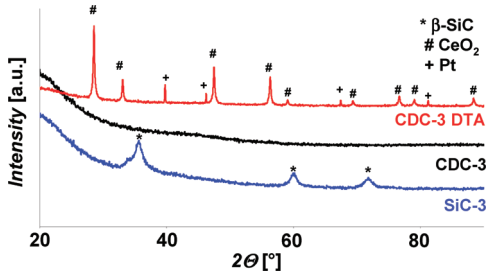

Figure 6. X-ray powder diffraction patterns of ceramic (SiC-3), CDC composites (CDC-3) and CeO_2/Pt structures after catalytic carbon combustion (CDC-3 DTA).

and platinum nanostructures. According to X-ray diffraction patterns, the cubic fluorite and the ccp-Pt phase remain and no sublimation effects of formed chloride structures were observed (ESI 8). However, strong sintering and aggregation occurs, because the crystallite sizes strongly increase from 25 nm (CeO_2) and 12 nm (Pt) to 247 and 222 nm, respectively. In contrast, no aggregation effects were detected for CDC composites (Figure 3, 4) demonstrating the templating effect of formed carbon matrix.

Thermogravimetric investigations coupled with differential thermal analysis (DTA/TG) were employed for investigation of thermal stability of CDC-X composites

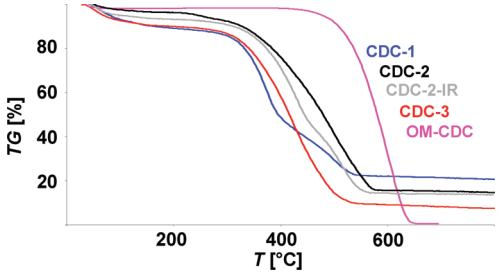

Figure 7. Thermogravimetric Investigations of CDC-X Composites and Mesoporous Reference Materials (CDC-meso) under Oxidative Conditions.

Table 3. Residual Masses of CeO_2/Pt Structures after Autocatalytic Carbon Combustion under Oxidative Conditions and Peak Temperatures Estimated by DTA of CDC Composites Synthesized at Different Pyrolysis and Chlorination Conditions

	CDC-				
	1	2	2-IR	3	OM-CDC[b]
$m_{residual}$ (%)[a]	20.7	14.7	13.6	7.4	< 0.01
$T_{min;DTA}$ [°C]	378/487	489	433/511	426	588

[a] Residual masses after calcination until 800 °C (CDC composites) and 700 °C (OM-CDC), respectively. [b] Ordered mesoporous CDC reference material (OM-CDC).

presented in Figure 7, Supporting Information 9, and Table 3 (Scheme 1, fifth step). In comparison to ordered mesoporous CDC reference material (OM-CDC), the metal-containing carbon materials have a significantly lower thermal stability because the temperature minimum in DTA analysis is shifted to 378 °C (CDC-1) compared to 588 °C (OM-CDC).[25] The latter is related to the catalytic activity of incorporated CeO_2/Pt nanoparticles in combustion of the CDC matrix. Similar results were also obtained in ceria nanoparticle promoted soot combustion.[38] The combustion temperature of CDC composites is dependent on the pyrolysis temperature (CDC-1, 378 °C; CDC-2, 489 °C). Additionally, for low-temperature pyrolyzed and short chlorination time a two-step combustion process is detectable, whereas for higher pyrolysis a broad DTA signal results. Hence, different catalysts to matrix interactions result in the composite materials dependent on the synthesis conditions. Furthermore, no complete mass reduction after calcination at 800 °C under air was detected for CDC-X composites compared to oxidation of OM-CDC reference material. XRD diffraction measurements of these solid residues reveal only crystalline ceria and platinum phases (Figure 6). However, the remaining masses reduce with increasing pyrolysis temperatures from 20.7 to 7.4 wt %. According to theoretical assumptions, a catalyst content of 14.7 wt % should result for the CDC composite material. The latter suggests possible sublimation effects of ceria and/or platinum at higher pyrolysis temperatures lowering the yield in resulting CDC composites.

The thermogravimetric results were confirmed by elementary analysis of carbonaceous composites since the cerium content decreases from 13.1 wt % after pyrolysis at 1200 °C (CDC-1) to 1.0 wt % for materials treated at 1500 °C (CDC-3). In contrast, the platinum content

slightly increases from 0.8 wt % (CDC-1) to 1.6 wt % (CDC-2/3) with higher pyrolysis temperatures. These results indicate preferential ceria sublimation at pyrolysis temperatures of 1350 and 1500 °C. In agreement to the above-discussed EDX analysis (Supporting Information 4) low silicon contents of less than 0.5 wt % were detected for all CDC composites, demonstrating the quantitative Si-removal during chlorination process.

Catalytic Tests. The catalytic activity of ceramic and carbonaceous composites, pyrolyzed at 1350 °C (SiC-2/CDC-2-IR-H), was tested in selective methane oxidation in fixed-bed reactor system under continuous oxygen deficient flow conditions. An oxygen deficit was chosen avoiding oxidation process of porous carbon systems and promoting the formation of carbon monoxide and hydrogen compounds (synthesis gas). Both materials offer catalytic activity since methane to carbon dioxide conversion can be observed upon 300 °C (Figure 8A). Increasing the reactor temperatures, upon 375 °C the hydrocarbon conversion of the carbon composite significantly increases while the activity of the ceramic material remains constant. The latter raise can be explained by the formation of carbon monoxide and hydrogen in subsiding reforming reactions for the metal containing carbide derived carbon material (Figure 8B). A further temperature raise up to 500 °C promotes also higher hydrogen yields (11%) and higher CO selectivity (37%). In contrast, no synthetic gas formation could be detected for the ceramic composite material. A possible explanation to the syn-gas formation for the CDC composites can be attributed to attractive methane interaction to the hydrophobic surface of the highly porous carbon matrix. In previous studies, we obtained high hydrocarbon uptakes for comparable, ordered mesostructured CDC materials.[46] Related to the presented carbon composite system, carbon dioxide and water that were formed during the first step by CeO_2/Pt nanoparticles catalyzed oxidation (Figure 8, oxidation reaction) can be reformed to relevant carbon monoxide and hydrogen by methane excess adsorbed at the ambient carbon matrix (Figure 8, reforming reactions). The presented metal containing CDC catalyst system offer comparable activities and selectivities to state of the art nanoscale CeO_2/Pt system with similar metal ratios measured under comparable conditions.[58] However, from economic and ecological aspects, significantly lower amounts of expensive transition and lanthanide metal compounds are necessary. Additionally, the catalytic active species is fixed in a stable and an environmental and biological more compatible carbon matrix.

During the selective methane oxidation the catalyst materials remain stable, since similar activities were obtained in second catalytic runs. Additionally, no oxidation process of the CDC material were analyzed, because the carbon balance as the molar ratio of gaseous gas species before and after the reaction stay constant for all studied temperatures. Furthermore, the CDC pore

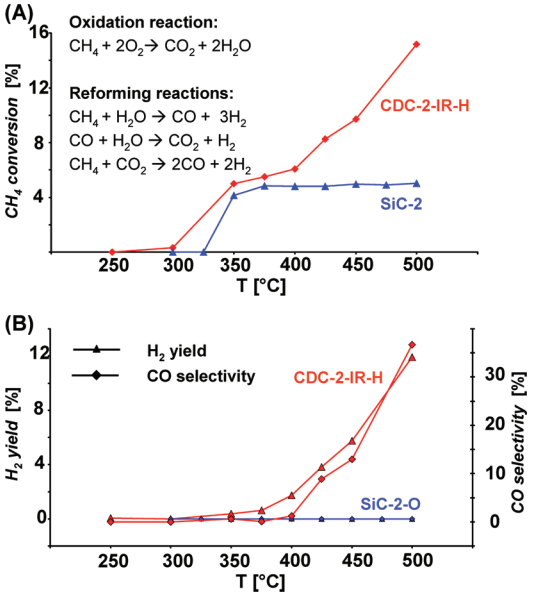

Figure 8. Catalytic activity of ceramic (SiC-2-O, blue) and carbonaceous composites (CDC-2-IR-H, red) under continuous flow conditions in (A) methane conversion and hydrogen yield and (B) CO selectivity, respectively, dependent on the reactor temperature.

structure remains intact during the catalytic process, since identical isotherm shapes and pore size distributions were obtained before and after oxidation reaction. The slight reduction in specific surface area and total pore volume can be ascribed to the quartz wool impurities of the fixed bed reactor.

In comparison to the thermal analysis presented in the previous chapter (Table 3), the higher stability of CDC composites as catalyst in methane oxidation can be ascribed to the significant lower oxygen concentration related to the gaseous hydrocarbon excess.

Conclusions

The present contribution provides a new strategy for the preparation of highly porous metal containing carbide derived carbon composites. The active platinum and ceria nanoparticles were incorporated in defined particle sizes using an inverse microemulsion method into the preceramic polycarbosilane structure. The metal-containing ceramic and carbon composite materials were obtained by pyrolysis and subsequent chlorination treatments. The pore size of resulting CDC materials can be precisely tuned from mainly microporous materials to high mesopore contents by pyrolysis temperatures. Additionally, a new chlorination method was applied using the IR-furnace technique yielding specific surface areas and pore volumes up to 1774 m^2/g and 1.79 cm^3/g, respectively which are significantly increased compared to conventional treatment conditions. In contrast to the unsupported CeO_2/Pt nanostructures the particle size and dispersion of catalytic active compounds in supported composites remains stable during pyrolysis and chlorination process verified by TEM and element sensitive mapping investigations. Additionally, catalytic activity and stability of CeO_2/Pt composites was demonstrated in

(58) Gaudillère, C.; Vernoux, P.; Mirodatos, C.; Caboche, G.; Farrusseng, D. *Catal. Today* **2010**, *157*, 263.

methane combustion. In comparison to the ceramic composites promoting the complete oxidation, carbonaceous materials induce the formation of energetically favorable carbon monoxide and hydrogen by catalytic reforming reactions. In comprehensive studies, the reproducibility of this synthesis strategy and the performance of the resulting catalyst systems in selective methane oxidation were demonstrated.

The introduced catalytic activity of these novel CeO_2/Pt-CDC composite materials can be interesting for a variety of other ceria-catalyzed reactions such as low-temperature water gas shift and denitrification reactions. Because of the modular design of used inverse microemulsion method, further active compounds like iron and ruthenium can be directly introduced. Additionally, the particle size and mass content can be controlled by the molar ratio of aqueous solution and surfactant.

Acknowledgment. The authors thank Dr. G. Auffermann (Max Planck Institute for Chemical Physics of Solids) for elementary analysis and DFG within the priority program SPP-1181 (Nanomat) for financial support.

Supporting Information Available: This material is available free of charge via the Internet at http://pubs.acs.org/.